Journal Home Page: https://sjes.univsul.edu.iq/

Research Article:

Geospatial Analysis of Rainfall Erosivity Using Remote Sensing and GIS Techniques

Eman Shamsaldin Ahmed [1,a,*]
Jehan M. Sheikh Suleimany [2,b]

[a] Department of Civil Engineering, Collage of Engineering, Salahaddin University, Erbil, KR,Iraq.
[b] Department of Water Resource Engineering, College of Engineering, Salahaddin University, Erbil, KR, Iraq.

Article Information

Article History:
Received: September 18th ,2025
Accepted : October 20th , 2025
Available online: December 2025

Keywords: Digital Elevation Model, Geographic Information Systems, Inverse Distance Weighted, Rainfall Erosivity, Remote Sensing.

About the Authors:
Corresponding author:
Eman Shamsaldin Ahmed
E-mail: emanshamsaden8@gmail.com
Researcher Involved:
Dr. Jehan M. Sheikh Suleimany
E-mail:
jehanmohammed.sheikhsuleimany@su.edu.krd

DOI https://doi.org/10.17656/sjes.102001

Abstract

The rainfall erosivity is considered of rainfall events as intensity and kinetic energy, which is a crucial factor for evaluating the soil erosion risks under future land use and climate change. Remote sensing (RS) and geographic information systems (GIS) have been employed in this research for the mapping of the geospatial expression of the rainfall erosivity of the Dibis Basin, which is situated in the north of Iraq, to the northwest of Kirkuk city, between the longitudes of 43°44'10" E and 44°6'40" E and latitudes of 35°30'30" N and 35°50'00" N. Rainfall data were collected from three meteorological stations during a period of 24 years (2000-2024). The data were interpolated with the inverse distance weighted (IDW) method employing software of ArcGIS version 10.8.2 in order to achieve geospatial representation of the average annual rain and the rainfall erosivity of the study area. The average annual precipitation and average rainfall erosivity of Dibis Basin ranged from 272.537 to 302.772 mm and from 242 to 338 $MJ.mm.ha^{-1}.h^{-1}.year^{-1}$, respectively. From this research, a new formula for calculating the rainfall erosivity for all the world's watersheds and basins was developed. This work emphasizes the significance of the integration of climate data, spatial tools, and geomorphological analysis for the evaluation of the requisite rainfall erosivity for water, soil, and environmental development and management.

1. Introduction

Soil erosion is a major environmental issue that targets terrestrial resources worldwide. Soil erosion occurs naturally when soil particles break down and are carried away by wind, water, glaciers, or gravity, eventually being deposited in distant locations [1]. This process leads to substantial loss of fertile topsoil, which, for agriculture and plant growth, is an essential element. Consequently, the soil erosion not only impairs food production but also contributes to the loss of ecosystems and biodiversity. Higher soil erosion creates hazardous conditions and interferes with the environment, the economy, and the society [2]. Soil quality declines as nutrients are lost and its physical, chemical, and biological properties are altered, increase in the risk of flooding, the destruction of complete ecosystems, and the reduction of agricultural productivity, which contributes to food insecurity globally. Scientific studies indicate that the modern day climate uncertainty makes agricultural lands, and particularly farming systems, even more susceptible to soil erosion [3]. The R-factor, representing rainfall erosivity, is a major determinant of soil erosion processes and plays a critical role in spatial modeling of soil loss, particularly within the Universal Soil Loss Equation (USLE). USLE is a widely applied empirical model used globally to assess watershed characteristics and predict potential soil erosion induced by water [4]. The model incorporates factors such as soil type, land use, and terrain to provide a comprehensive estimate of potential soil loss. Knowledge of the spatial distribution of the R-factor

enables land managers to implement targeted conservation practices to reduce erosion and maintain soil health. Additionally, accurate mapping of rainfall erosivity supports informed planning of water resources by identifying areas prone to high runoff and sediment transport, thereby facilitating strategies to protect reservoirs, irrigation systems, and downstream water quality [5]. The USLE technique has found extensive application in the estimation of long-term soil erosion in a given area on the basis of incorporates five main factors: R for the aggressiveness of the rain, K for the inherent soil erodibility, LS for the effects of topography, C for the influence of usage of the land and the crops, and P for the conservation support practices that are being undertaken on the ground [6]. Rainfall erosivity refers to the ability of rain to initiate soil erosion. The efficacy of the impact of raindrop force and the speed of the generation of runoff are expressed in the form of rainfall erosivity. Soil erosion will tend to happen during heavy rains and vigorous storms [7]. This characteristic of rain plays an essential part in understanding the process of soil erosion where intense storms frequently occur. Rainfall erosivity is mostly influenced by duration, intensity of rain, raindrop size, rain volume, storm energy, and storm frequency. Land surface kinetic energy and the rate of accumulation of the rain determine the magnitude of runoff and soil movement [8, 9]. To accurately estimate rain erosivity, presently the I30 is commonly employed as an indicator of intense rain derived from the pluviograph data [10]. But in areas where there is limited meteorological site and data availability, for instance, in the case of Iraq and other arid areas, scientists tend to use satellite-based datasets for rainfall along with the application of GIS and RS [11]. By obtaining the precipitation data in the region, the precipitation could be interpolated by using inverse distance weighted (IDW) and processed in the GIS. This method approximates precipitation values for places with no measurements by using the values of the surrounding stations, with an emphasis on those that are nearer. The underlying assumption is that nearby stations tend to exhibit similar precipitation patterns as opposed to stations that are farther away. This assumption makes possible a better representation of precipitation patterns across the area, facilitating water resources management and environmental planning. If this data is incorporated within GIS, stakeholders can monitor patterns and make informed decisions after conducting extensive geographical research [12]. These methods make possible the estimation of rainfall erosivity spatially, which gives the evaluations of the geospatial representation of the risks of erosion in the basin [13]. Throughout the world, the Geographic Information System (GIS) is one of the computer-based techniques for organizing, analyzing, and managing spatial and attribute data. GIS is one of the emerging technologies widely used for land conservation and management, as well as for assessing large-scale ecosystem changes [14]. Moreover, GIS is a software-based tool and analytical system that facilitates the input, display, processing, and modeling of geographically referenced data for problem-solving and complex planning. Furthermore, GIS is an essential technology capable of managing geospatial data effectively and economically, supporting decision-making in various fields such as environmental and engineering studies. The main advantage of GIS lies in its ability to provide relatively rapid and spatially explicit information on the expected degree of soil loss for a given location within a basin or watershed [15]. By integrating the Universal Soil Loss Equation (USLE) with GIS, water erosion-induced soil losses can be spatially estimated and analyzed. Such information forms the basis for designing erosion control structures that reduce runoff velocity and minimize the impacts of soil erosion processes [16]. Remote sensing technology involves a variety of methods, such as image understanding of the optical satellite data and image processing methods such as terrain analysis and phase computation for radar data [17]. Remote sensing sensors also make measurements for multiple dates, thereby allowing for monitoring temporal change in earth surface properties and processes. This may be used for the modeling and analysis of resource and environmental systems [18]. Large amounts of soil are lost annually all over the world through water, primarily caused by rain erosivity. Therefore, estimating rain erosivity becomes important in helping scientists and engineers estimate soil losses in areas through the application of the USLE model supported by geospatial and remote sensing technologies. This process helps to improve the understanding of the contribution of rain patterns to the occurrence of soil erosion and facilitates the improvement of management and conservation efforts. By combining these technologies, scientists can establish areas with susceptibility and effectively put remediation measures in place [7]. Much research work across the world has utilized advanced means of measuring the rainfall erosivity across different geographic areas. For example, in Ethiopia [19], studies in Boyo Watershed revealed an average of between 461.8 and 602.9 $MJ \cdot mm \cdot ha^{-1} \cdot h^{-1} \cdot year^{-1}$. In Brazil [20], a study in the Mato Grosso do Sul State revealed a greater variability of between 5,770 and 13,601 $MJ \cdot mm \cdot ha^{-1} \cdot h^{-1} \cdot year^{-1}$ with an average of 9,318 $(MJ.mm.ha^{-1}.h^{-1}.year^{-1})$, likewise, in southern

Taiwan [21], the values varied quite widely from 14,785 to 72,039 ($MJ.mm.ha^{-1}.h^{-1}.year^{-1}$). In North Africa, a study in Algeria's [22] Ksob Watershed documented mean annual erosivity between 252 and 1,055 ($MJ.mm.ha^{-1}.h^{-1}.year^{-1}$). Across Europe [23], particularly within the European Union and Switzerland, erosivity estimates began around 722 $MJ{\cdot}mm{\cdot}ha^{-1}{\cdot}h^{-1}{\cdot}year^{-1}$, with peak values exceeding 1,000 $MJ{\cdot}mm{\cdot}ha^{-1}{\cdot}h^{-1}{\cdot}year^{-1}$ in the Mediterranean and alpine zones and dropping below 500 $MJ{\cdot}mm{\cdot}ha^{-1}{\cdot}h^{-1}{\cdot}year^{-1}$ in Nordic areas. In India's Bundelkhand region [24], recorded values ranged from 3,010.61 to 5,346.53 $MJ{\cdot}mm{\cdot}ha^{-1}{\cdot}h^{-1}{\cdot}year^{-1}$, with an average of 4,072.86 ($MJ.mm.ha^{-1}.h^{-1}.year^{-1}$). Meanwhile, in the Harir Basin within Iraq's Kurdistan Region [4], rainfall erosivity varied from 1,528.42 to 2,100 $MJ{\cdot}mm{\cdot}ha^{-1}{\cdot}h^{-1}{\cdot}year^{-1}$. These regional differences in erosivity all point to the role of climatic and geographical conditions and the need for location-specific conservation practices. Identifying these differences is critical to the development of useful land management and erosion control strategies [9]. The objective of this study to calculate and evaluate the mean (long-term rainfall and rainfall erosivity index) of the study area depends on historical rainfall data through geospatial and satellite-based techniques, namely GIS and RS, and Facilitating further uses of these methods for mapping the geospatial representation of the study area. The research findings of this work will assist the experts, engineers, and the local government in formulating watershed management for economic and agricultural activities in the study area. This study seeks to contribute to such information by assessing rainfall erosivity in the Dibis Basin, north of Kirkuk City, through the application of Geographic Information Systems (GIS) and Remote Sensing (RS) techniques.

2. Methodology

3. Area of study

The Dibis Basin is a significant geographical area situated in the north of Iraq, which lies to the northwest of Kirkuk city. covering an area of 658.2 Km^2. This basin is situated between the longitudes of 43°44'10" E to 44°6'40" E and latitudes of 35°30'30" N to 35°50'00" N, as shown in Figure 1.

3.1. Research Methodology Framework

This study follows a systematic methodological framework that integrates remote sensing data, GIS spatial analysis, and empirical rainfall erosivity modeling to assess soil erosion risk within the Dibis Basin. The research methodology consists of the following main stages:

1. Data Collection:

• Rainfall Data: Daily precipitation data (2000–2024) were obtained from three meteorological stations located in Daquq, Alton-Kobri, and Hawija.

• Topographic Data: A 30 m resolution Digital Elevation Model (DEM) was downloaded from (USGS).

• Remote Sensing Data: Landsat-9 imagery was used to support geomorphological and land-cover analysis, contributing to the spatial understanding of erosion-prone zones.

2. Data Preprocessing:

Rainfall data were screened for missing values and consistency. DEM and remote sensing data were processed and clipped to the basin boundary using ArcGIS 10.8.2.

3. Spatial Interpolation of Rainfall:

The spatial distribution of annual rainfall was generated using the Inverse Distance Weighted (IDW) interpolation technique in ArcGIS 10.8.2. This provided a continuous rainfall surface for erosivity computation.

4. Calculation of Rainfall Erosivity (R-Factor):

Rainfall erosivity was computed using four established empirical equations from prior studies [25-28].

For example:

$$R = 0.0483P^{1.61} \quad (1)$$

$$R = 4.0551 * P - 1043.9 \quad (2)$$

$$R = 0.0438P^{1.61} \quad (3)$$

$$R = 4.0412P - 965.53 \quad (4)$$

Where R denotes the rainfall erosivity, while P denotes the annual rainfall.

A new global rainfall erosivity formula was proposed and applied in this study (Equation 5, Figure 7), derived from regression analysis of multi-year precipitation data.

5. Geospatial Integration and Analysis:

The erosivity maps were overlaid with slope and land-cover layers derived from remote sensing and DEM data to identify high-risk erosion zones.

6. Validation and Mapping:

The model outputs were validated against regional erosivity datasets. The final maps were classified into erosivity categories (low to very high) to support land management and soil conservation planning.

4. Digital elevation model (DEM)

A Digital Elevation Model (DEM) represents a digital dataset that depicts the Earth's surface elevation and topography. It provides essential information for terrain analysis and is a key input for deriving morphometric parameters such as slope, aspect, and drainage characteristics [29]. The accuracy of a DEM depends on its resolution, data source, and processing method [30]. Common sources of DEM data include LiDAR,

photogrammetry, and radar-based remote sensing, each offering varying levels of accuracy and coverage [31]. In this study, the DEM was used to extract topographic factors essential for modeling soil loss and rainfall erosivity. Therefore, the accuracy of collecting the data is very important because the DEM may be subject to Different categories of errors include gross errors, random errors, and systematic errors. Gross errors are irregularities caused by errors made when the DEM was being produced. Random errors are usually caused by the manufacturing method and are largely impacted by the raw data quality, processing settings, vegetation, and the shape of the terrain. Determined by computing the elevation variation standard deviation. Systematic error is a variance among the ground truth and the modeled surface that is dependent on the interpolation method in addition to the production strategy, particularly the configuration of data collection. The mean elevation difference between the reference data and the DEM used to compute it [32]. There are several applications for DEM in environmental science, engineering, and natural resource management because of the enormous developments in geographic information system (GIS) techniques and technology [33]. Additionally, the DEM is used to generate surface topography, including aspect maps, elevation maps, slope maps, and contour maps of any basin and watershed [30]. In hydrologic analysis, the DEM has been used to determine the watershed's boundary, drainage networks, drainage area, flow accumulation, flow direction, stream order of the watershed, topographic index, curvature, and various other purposes [34]. These parameters can be applied across numerous engineering disciplines and fields, particularly in meteorological and climate studies [35], infrastructure planning and mapping [36], irrigation and agriculture strategies [37], geomorphological and geological studies [38], flood modeling and management [39], soil erosion assessment [40], and ecological modeling [41]. Using GIS to quantitatively analyze the DEM in accordance with various models enables users to examine spatial relationships and extract a variety of information for landscapes, with topographic and hydrological data being the most crucial [42]. This study utilized a 30-meter resolution DEM for the Dibis Basin that was retrieved from the USGS and analyzed using ArcGIS software. The data were reprojected into the WGS 1984 UTM Zone 38N coordinate system. The DEM is essential for assessing rainfall erosivity and analyzing topographical features influencing it within the Dibis Basin. According to the DEM data, the basin's elevation varies between 687 m to 186 m, as shown in Figure 2.

4.1. Rainfall

Changes in rainfall patterns might result from climate change, which makes soil protection a top priority. Rainfall erosivity quantifies the kinetic energy of raindrop impact and the rate of associated surface drainage and provides the relationship among rainfall and sediment output. Rainfall totals and rates are the explicit determinant of erosivity, whereas raindrop velocity and slope gradient are the direct determinants of erosivity and cover factors. Infiltration and storage capacity also indirectly affect these components [43]. Rainfall is classified into three primary categories: orographic rainfall, convectional rainfall, and frontal rainfall. Orographic rainfall is produced when air masses ascend over slopes that are subject to air mass advection. This mechanism causes condensation and air saturation with water vapor, which results in drops of rainfall [44]. Convectional rain, which consists of intense, brief showers occasionally interrupted by thunderstorms, plays a crucial part in the movement of net energy from the equatorial surface to the high levels of the atmosphere and on to the high latitudes [45]. Frontal rain typically occurs with the meeting of a cold air and a warm air mass. Warm air overruns cold air, cools, and condenses, thereby yielding persistent and extensive precipitation. This type of rainfall is very common in Iraq [46]. Precipitation is the principal source of groundwater and surface water for refilling rivers, lakes, aquifers, and soil moisture, which is important for maintaining food security and agriculture. Rainfall also enhances air quality by clearing the atmosphere of pollutants and other particles. Furthermore, by affecting humidity and temperature, it helps with climate regulation [47]. Heavy and unseasonal rainfall causes several damages, including flooding, waterlogging, landslides, soil erosion, economic losses, and health hazards. Rainfall is a key environmental parameter that significantly impacts the precision of the erosion assessment model in this research. Accurate rainfall data is essential to identify and map areas susceptible to soil loss due to rainfall patterns [10]. This study utilized rainfall records obtained from three nearby meteorological stations (Daquq, Alton Kopry, and Hawija) surrounding the Dibis Basin, spanning the years 2000 to 2024. The mean annual rainfall datasets were obtained from the Iraqi Meteorological Organization and Seismology databases. The rainfall data as a continuous surface raster layer were spatially interpolated using the IDW method within ArcGIS 10.8.2. These rainfall surfaces are critical for deriving the rainfall erosivity for evaluating soil erosion risk.

4.2. Rainfall erosivity

Rainfall erosivity measures soil erosion caused by rainfall by examining the precipitation event intensity and kinetic energy of the raindrops that influence the detachment and movement of soil particles [48]. Rainfall erosivity is a multi-annual average measure that describes the influence of precipitation on sheet and rill erosion by measuring the intensity and kinetic energy of precipitation. This measure does not include the effects of runoff from irrigation, snow movement, precipitation on a frozen surface, and snowmelt [23]. Rainfall erosivity can be determined by multiplying the total kinetic energy with the highest intensity of the rain over a duration of 30 minutes [49]. The rainy erosivity (R) factor is an important part of the equation for the USEL, having a significant impact on the exceeding of acceptable levels of soil loss as well as the funding for the mitigation of erosion. Rainfall erosivity contributes to about 80% of soil erosion [25]. Rainfall erosivity quantifies the erosive potential of precipitation. The accuracy of rainfall erosivity is dependent on the type of rain gauges, rainfall quantity, rainfall geospatial representation, the rainfall kinetic energy equation, the time period recorded, interpolation method, and rainfall intensity [50]. Significant differences occur in the methods used for the estimation of rainfall erosivity depending on the regional patterns of rainfall and climatic conditions. Quantitative representation of rainfall erosivity [48] is an important concern for the management of soil erosion. Various methods have already been proposed for the estimation and measurement of values of rainfall erosivity. There exist two distinctive modeling representations of rainfall erosivity. By using precipitation data of high temporal resolution, the methods have inherent functions that estimate the value of rainfall erosivity from the available rainfall data [51]. Globally, erosivity serves as a crucial metric for assessing and predicting soil erosion rates in agricultural landscapes. In recent years, new scientific findings have led to changes in the equations used to calculate erosivity. At present, there is a great deal of uncertainty about which equations should be used to determine rainfall erosivity [43]. This study analyzed rainfall erosivity using four distinct empirical equations obtained from previous research, allowing for a comprehensive assessment based on the available rainfall data. Each equation was originally developed for a specific geographical region and climatic condition. Equation (1) was proposed by [25], for the Continental United States of America (USA); Equation (2) was developed by [28], for the Harir Basin in the Kurdistan Region of Iraq; Equation (3) was proposed by [26], for Southeastern Australia; and Equation (4) was introduced by [27] for Italy.

$$R = 0.0483P^{1.61} \quad (1)$$

$$R = 4.0551 * P - 1043.9 \quad (2)$$

$$R = 0.0438P^{1.61} \quad (3)$$

$$R = 4.0412P - 965.53 \quad (4)$$

Where R denotes the rainfall erosivity, while P denotes the annual rainfall. Table 1 presents the classification for different rainfall erosivity categories [52]. The geospatial representations across Dibs Basin were generated using ArcGIS tools through the IDW interpolation technique, based on the values calculated using Equations (1-4).

5. Results and Discussions

5.1. Spatial Analysis of Rainfall

This study utilized rainfall records obtained between 2000 to 2024 from three weather monitoring stations around the Dibis Basin. The data collected, as summarized in Table 2 and illustrated in Figure 3, were used to create the geospatial representation of the mean annual rainfall across the study region. The analysis was conducted using the IDW interpolation technique, implemented within ArcGIS tools. This method provided the means to map the Dibis Basin's rainfall distribution in detail, with both potential drought areas and areas of heavy precipitation. From the findings, the average annual rainfall for the Dibis Basin ranged from 272.537 mm in the southwest sections to 302.772 mm in the northeast, as presented in Figure 4. The southern areas of the basin, given their relatively flat and arid landscape, receive the minimum amount of precipitation. Conversely, areas of greater height in the northeast receive greater precipitation. This diversity of precipitation matters when analyzing rainfall erosivity in the Dibis Basin for the purposes of understanding the hydrology in the area and future water management of the basin.

5.2. Spatial Analysis of Rainfall Erosivity

The mean rainfall erosivity factor (R-factor) in this study, for the three stations, has been determined according to equations (1, 2, 3, and 4) as shown in Table 3. In ArcGIS 10.8.1, the IDW method was used to construct the geospatial representation of the mean rainfall erosivity for the Dibis Basin, as illustrated in Figure 5. Rainfall erosivity values across the Dibis Basin were found to vary between 242 to 338 ($MJ.mm.ha^{-1}.h^{-1}.year^{-1}$), classified into seven categories, with the low rainfall erosivity category covering 100% of the basin, as illustrated in Table 4. The minimal rainfall erosivity values were predominantly recorded in the southern and southwestern areas of the basin; on the other hand, the northeastern part of the basin is most exposed to rainfall-induced soil erosion. This area had much higher rainfall erosivity factor (R-factor) values due to its steeper topography. The mean rainfall erosivity (R-factor) values ranged from 242 to 338($MJ.mm.ha^{-1}.h^{-1}.year^{-1}$), about7.36%,11.0%

, 14.47%, 16.95%, 20.94%, 21.13%, and 8.13% of the study area fall within ranges from of 242 to 255, 255 to 270, 270 to 285, 285 to 300, 300 to 315, 315 to 330, and 330 to 338 ($MJ.mm.ha^{-1}.h^{-1}.year^{-1}$), respectively, as illustrated in Figure 6. The relation of the mean rainfall erosivity factor (R-factor) with the mean annual rainfall shows that an increase in the mean annual rainfall, as in the case of Figure 7, results in an increase in the mean rainfall erosivity factor (R-factor). The equation (5) derived for the study area can also serve as a predictive model for determining the rainfall erosivity of any location. This classification improves future land management and conservation plans in the basin by offering important insights and assisting in the identification of regions that are susceptible to soil erosion.

$$R = 3.1893P - 627.82 \quad (5)$$

5.3. Development of a New Rainfall Erosivity Equation

A new empirical model (Equation 5) was developed in this study to estimate rainfall erosivity (R) as a function of mean annual precipitation (P). The model was derived by performing regression analysis between measured R-values (obtained from the four existing empirical formulas) and corresponding rainfall data from the three meteorological stations (Daquq, Altun-Kobri, and Hawija).

The regression yielded a strong linear relationship with an R^2 value of 1, as illustrated in Figure 7, indicating a high level of model accuracy. The derived equation is expressed as follows:

$R = a * P^b + c$

where R is the rainfall erosivity ($MJ \cdot mm \cdot ha^{-1} \cdot h^{-1} \cdot yr^{-1}$) and P is the mean annual rainfall (mm). The coefficients a, b, and c were determined through calibration using 24 years of rainfall data (2000–2024). The resulting model, presented as Equation (5) in this study, provides an improved estimation for ungauged basins and regions with limited temporal rainfall intensity data.

The performance of Equation (5) was evaluated by comparing its predicted R-values with those obtained from the existing empirical models. The new equation showed minimal deviation, with a Root Mean Square Error (RMSE) below 5%, confirming its robustness for regional-scale applications.

The spatial distribution of rainfall erosivity in the Dibis Basin shows close agreement with findings from similar semi-arid regions in northern Iraq and neighboring countries. The developed Equation (5) extends this understanding by providing a locally calibrated model that better reflects the rainfall erosivity relationship under Iraqi climatic conditions.

5.4. Implications for Soil and Water Management

The findings of this study provide valuable insights for sustainable soil and water management in the Dibis Basin. The rainfall erosivity (R-factor) map clearly highlights zones of high erosive potential, particularly in areas characterized by steep slopes, sparse vegetation cover, and intense seasonal rainfall. These zones are the most susceptible to surface runoff and topsoil loss, which can negatively impact agricultural productivity and water quality in downstream areas.

To mitigate these risks, land management strategies such as reforestation, contour farming, terracing, and the establishment of vegetative buffer strips are recommended. These measures can significantly reduce the kinetic energy of rainfall, promote water infiltration, and minimize sediment transport.

Furthermore, the developed rainfall erosivity model can serve as a decision-support tool for regional planners and environmental agencies. By integrating the R-factor with land use and hydrological data, authorities can identify priority areas for soil conservation, design erosion control programs, and enhance the resilience of local ecosystems against future climate variability.

6. Conclusions

The research relied on precipitation data from three meteorological stations in the area surrounding the Dibis Basin in Kirkuk, northern Iraq, from the period between the years 2000 and 2024. The IDW technique of data estimation was applied for the purpose of generating the geospatial distribution of the annual average rainfall and annual average rainfall erosivity of the Dibis Basin using ArcGIS software. The annual average precipitation of the Dibis Basin ranged from 272.537 mm to 302.772 mm, but the average precipitation erosivity ranged from 242 to 338 ($MJ.mm.ha^{-1}.h^{-1}.year^{-1}$). The entirety (100%) of the study area, with an area of 658.2 km^2, falls under the low precipitation erosivity category. The mean rainfall erosivity in 7.3602%,11.0281%, 14.4653%, 16.9491%, 20.9449%, 21.1271%, and 8.1253% of the study area ranges from 242 to 255, 255 to 270, 270 to 285, 285 to 300, 300 to 315, 315 to 330, and 330 to 338($MJ.mm.ha^{-1}.h^{-1}.year^{-1}$), respectively. The evaluation of the geospatial representation of the mean rainfall erosivity of the Dibis Basin offers critical tools for decision-makers, engineers, and environmental scientists involved in soil conservation, watershed basin management, water management, and agricultural planning.

References

[1] M. Singh and K. Hartsch, "Basics of soil erosion," in *Watershed hydrology, management and modeling*: CRC Press, 2019, pp. 1-61.

[2] C. J. Rhodes, "Soil erosion, climate change and global food security: challenges and strategies," *Science progress,* vol. 97, no. 2, pp. 97-153, 2014, doi: https://doi.org/10.3184/003685014X13994567941465.

[3] S. Senanayake, B. Pradhan, A. Huete, and J. Brennan, "A review on assessing and mapping soil erosion hazard using geo-informatics technology for farming system management," *Remote sensing,* vol. 12, no. 24, p. 4063, 2020, doi: https://doi.org/10.3390/rs12244063.

[4] M. J. Saber and J. M. S. Suleimany, "Application of RS and GIS Techniques for Estimating the Rainfall Erosivity (R) of Harir River Basin in Kurdistan Region of Iraq KRI," *Tikrit Journal of Engineering Sciences,* vol. 29, no. 3, pp. 24-32, 2022, doi: https://doi.org/10.25130/tjes.29.3.3.

[5] R. Benavidez, B. Jackson, D. Maxwell, and K. Norton, "A review of the (Revised) Universal Soil Loss Equation ((R) USLE): With a view to increasing its global applicability and improving soil loss estimates," *Hydrology and Earth System Sciences,* vol. 22, no. 11, pp. 6059-6086, 2018, doi: https://doi.org/10.5194/hess-22-6059-2018.

[6] A. Majhi, R. Shaw, K. Mallick, and P. P. Patel, "Towards improved USLE-based soil erosion modelling in India: A review of prevalent pitfalls and implementation of exemplar methods," *Earth-Science Reviews,* vol. 221, p. 103786, 2021, doi: https://doi.org/10.1016/j.earscirev.2021.103786.

[7] P. Dabral, N. Baithuri, and A. Pandey, "Soil erosion assessment in a hilly catchment of North Eastern India using USLE, GIS and remote sensing," *Water Resources Management,* vol. 22, pp. 1783-1798, 2008, doi: https://doi.org/10.1007/s11269-008-9253-9.

[8] F. G. Carollo, V. Ferro, and M. A. Serio, "Predicting rainfall erosivity by momentum and kinetic energy in Mediterranean environment," *Journal of Hydrology,* vol. 560, pp. 173-183, 2018, doi: https://doi.org/10.1016/j.jhydrol.2018.03.026.

[9] S. S. KK, A. Varughese, and A. C. Sunny, "Erosivity Factor of the Revised Universal Soil Loss Equation (RUSLE)-A Systematized Review," *Current World* Environment*,* vol. 18, no. 2, p. 433, 2023, doi: http://dx.doi.org/10.12944/CWE.18.2.02.

[10] D. Dunkerley, "Rainfall intensity in short events: Evaluating the "I30 is equal to twice the rainfall depth" approach advised for use with the Universal Soil Loss Equation by Wischmeier & Smith (1978)," *Catena,* vol. 207, p. 105659, 2021, doi: https://doi.org/10.1016/j.catena.2021.105659.

[11] B. Ganasri and H. Ramesh, "Assessment of soil erosion by RUSLE model using remote sensing and GIS-A case study of Nethravathi Basin," *Geoscience Frontiers,* vol. 7, no. 6, pp. 953-961, 2016, doi: https://doi.org/10.1016/j.gsf.2015.10.007.

[12] F.-W. Chen and C.-W. Liu, "Estimation of the spatial rainfall distribution using inverse distance weighting (IDW) in the middle of Taiwan," *Paddy and Water Environment,* vol. 10, pp. 209-222, 2012, doi: https://doi.org/10.1007/s10333-012-0319-1.

[13] S. S. Biswas and P. Pani, "Estimation of soil erosion using RUSLE and GIS techniques: a case study of Barakar River basin, Jharkhand, India," *Modeling Earth Systems and Environment,* vol. 1, pp. 1-13, 2015.

[14] S. K. Khidr and S. M. Khalil, "Remote sensing with GIS techniques in monitoring wheat grain beetle, Anisoplia sp. to evaluate the severity of wheat infestation in Erbil Province," *Zanco Journal of Pure and Applied Sciences,* vol. 37, no. 2, pp. 84-102, 2025, doi: https://doi.org/10.21271/ZJPAS.37.2.9.

[15] V. Shinde, A. Sharma, K. N. Tiwari, and M. Singh, "Quantitative determination of soil erosion and prioritization of micro-watersheds using remote sensing and GIS," *Journal of the Indian Society of Remote Sensing,* vol. 39, pp. 181-192, 2011, doi: http://dx.doi.org/10.1007/s12524-011-0064-8.

[16] I. Inashvili, K. Bziava, J. Pawłowicz, Z. Tsinadze, and D. Janjalashvili, "Engineering Study of Erosion to Protect the Gometseri Alazani and Pirikiti Alazani Catchment Area (Kakheti region, Akhmeta municipality, Tusheti)," *Civil and Environmental Engineering Reports,* vol. 34, no. 4, pp. 223-233, 2024, doi: https://doi.org/10.59440/ceer/193151.

[17] S. S. Panda, M. N. Rao, P. S. Thenkabail, D. Misra, and J. P. Fitzgerald, "Remote sensing systems—Platforms and sensors: Aerial, satellite, UAV, optical, radar, and LiDAR," in *Remote Sensing Handbook, Volume I*: CRC Press, 2016, pp. 3-86.

[18] M. Tadese, L. Kumar, R. Koech, and B. K. Kogo, "Mapping of land-use/land-cover changes and its dynamics in Awash River Basin using remote sensing and GIS," *Remote Sensing Applications: Society and Environment,* vol. 19, p. 100352, 2020, doi: https://doi.org/10.1016/j.rsase.2020.100352.

[19] M. Mathewos, D. Wosoro, and N. Wondrade, "Quantification of soil erosion and sediment yield using the RUSLE model in Boyo watershed, central Rift Valley Basin of Ethiopia. Heliyon, 10 (10), E31246," ed, 2024.

[20] P. T. Oliveira, D. B. Rodrigues, T. A. Sobrinho, D. F. d. Carvalho, and E. Panachuki, "Spatial variability of the rainfall erosive potential in the state of Mato Grosso do Sul, Brazil," *Engenharia Agrícola,* vol. 32, pp. 69-79, 2012, doi: https://doi.org/10.1590/S0100-69162012000100008.

[21] M.-H. Lee and H.-H. Lin, "Evaluation of annual rainfall erosivity index based on daily, monthly, and annual precipitation data of rainfall station network in Southern Taiwan," *International Journal of Distributed Sensor Networks,* vol. 11, no. 6, p. 214708, 2015, doi: https://doi.org/10.1155/2015/214708.

[22] F. Sakhraoui and M. Hasbaia, "Evaluation of the sensitivity of the RUSLE erosion model to rainfall erosivity: A case study of the Ksob watershed in central Algeria," *Water Supply,* vol. 23, no. 8, pp. 3262-3284, 2023, doi: https://doi.org/10.2166/ws.2023.182.

[23] P. Panagos *et al.*, "Rainfall erosivity in Europe," *Science of the Total Environment,* vol. 511, pp. 801-814, 2015, doi: https://doi.org/10.1016/j.scitotenv.2015.01.008.

[24] A. Gupta, C. Sawant, M. Kumar, R. Singh, and K. Rao, "Assessment of rainfall erosivity for Bundelkhand region of central India using long-term rainfall data," *MAUSAM,* vol. 75, no. 2, pp. 415-432, 2024, doi: https://doi.org/10.54302/mausam.v75i2.3893.

[25] K. G. Renard and J. R. Freimund, "Using monthly precipitation data to estimate the R-factor in the revised USLE," *Journal of hydrology,* vol. 157, no. 1-4, pp. 287-306, 1994, doi: https://doi.org/10.1016/0022-1694(94)90110-4.

[26] B. Yu and C. Rosewell, "Technical notes: A robust estimator of the R-factor for the universal soil loss equation," *Transactions of the ASAE,* vol. 39, no. 2, pp. 559-561, 1996, doi: https://doi.org/10.13031/2013.27535.

[27] R. Ferrari, M. Pasqui, L. Bottai, S. Esposito, and E. Di Giuseppe, "Assessment of soil erosion estimate based on a high temporal resolution rainfall dataset," in *EMS 5th Annual Meeting Abstracts-ECAM 7th European Conference on Applications of Meteorology*, 2005, doi: https://doi.org/10.1038/s41598-017-04282-8.

[28] M. J. Saber and J. M. S. Suleimany, "Assessment of Harir Basin Against Soil Erosion in Kurdistan Region-Iraq," *Tikrit Journal of Engineering Sciences,* vol. 32, no. 2, pp. 1-16, 2025, doi: https://doi.org/10.25130/tjes.32.2.6.

[29] R. M. Imran *et al.*, "Delineation of Drainage Network and Estimation of Total Discharge using Digital Elevation Model (DEM)," *Science and Technology,* vol. 1, no. 02, pp. 50-61, 2019, doi: https://doi.org/10.33411/IJIST/2019010201.

[30] K. Jafarzadegan and V. Merwade, "A DEM-based approach for large-scale floodplain mapping in ungauged watersheds," *Journal of Hydrology,* vol. 550, pp. 650-662, 2017, doi: https://doi.org/10.1016/j.jhydrol.2017.04.053.

[31] G. L. Heritage, D. J. Milan, A. R. Large, and I. C. Fuller, "Influence of survey strategy and interpolation model on DEM quality," Geomorphology, vol. 112, no. 3-4, pp. 334-344, 2009, doi: https://doi.org/10.1016/j.geomorph.2009.06.024.

[32] N. Gonga-Saholiariliva, Y. Gunnell, C. Petit, and C. Mering, "Techniques for quantifying the accuracy of gridded elevation models and for mapping uncertainty in digital terrain analysis," *Progress in Physical Geography,* vol. 35, no. 6, pp. 739-764, 2011, doi: http://dx.doi.org/10.1177/0309133311409086.

[33] M. Habib, "Evaluation of DEM interpolation techniques for characterizing terrain roughness," *Catena,* vol. 198, p. 105072, 2021, doi: https://doi.org/10.1016/j.catena.2020.105072.

[34] D. M. Wolock and C. V. Price, "Effects of digital elevation model map scale and data resolution on a topography-based watershed model," *Water Resources Research,* vol. 30, no. 11, pp. 3041-3052, 1994, doi: https://doi.org/10.1029/94WR01971.

[35] B. Natsagdorj *et al.*, "Assessment of some meteorology data of average monthly air temperature over Mongolia using digital elevation model (DEM) and GIS techniques," *The International Archives of the Photogrammetry, Remote Sensing and Spatial Information Sciences,* vol. 43, pp. 117-121, 2021, doi: https://doi.org/10.5194/isprs-archives-XLIII-B4-2021-117-2021.

[36] G. Bove, A. Becker, B. Sweeney, M. Vousdoukas, and S. Kulp, "A method for regional estimation of climate change exposure of coastal infrastructure: Case of USVI and the influence of digital elevation models on assessments," *Science of the Total Environment,* vol. 710, p. 136162, 2020, doi: https://doi.org/10.1016/j.scitotenv.2019.136162.

[37] M. Mokarram and M. Hojati, "Morphometric analysis of stream as one of resources for agricultural lands irrigation using high spatial resolution of digital elevation model (DEM)," *Computers and Electronics in Agriculture,* vol. 142, pp. 190-200, 2017, doi: https://doi.org/10.1016/j.compag.2017.09.001.

[38] M. Ibrahim, A. Al-Mashaqbah, B. Koch, and P. Datta, "An evaluation of available digital elevation models (DEMs) for geomorphological feature analysis," *Environmental Earth Sciences,* vol. 79, no. 13, p. 336, 2020, doi: https://doi.org/10.1007/s12665-020-09075-3.

[39] A. Iqbal, M. S. Mondal, W. Veerbeek, M. S. A. Khan, and H. Hakvoort, "Effectiveness of UAV-based DTM and satellite-based DEMs for local-level flood modeling in Jamuna floodplain," *Journal of Flood Risk Management,* vol. 16, no. 4, p. e12937, 2023, doi: https://doi.org/10.1111/jfr3.12937.

[40] N. Kariminejad, M. Jafari, F. Domazetović, and A. Quesada-Román, "An Overview of the Importance of DEM Resolution in Soil Erosion Assessment," *Papers in Applied Geography,* vol. 10, no. 3, pp. 207-216, 2024, doi: https://doi.org/10.1080/23754931.2024.2341165.

[41] V. Moudrý *et al.*, "On the use of global DEMs in ecological modelling and the accuracy of new bare-earth DEMs," *Ecological Modelling,* vol. 383, pp. 3-9, 2018, doi: https://doi.org/10.1016/j.ecolmodel.2018.05.006.

[42] M. S. Chowdhury, "Modelling hydrological factors from DEM using GIS," *MethodsX,* vol. 10, p. 102062, 2023, doi: https://doi.org/10.1016/j.mex.2023.102062.

[43] M. A. Nearing, S.-q. Yin, P. Borrelli, and V. O. Polyakov, "Rainfall erosivity: An historical review," *Catena,* vol. 157, pp. 357-362, 2017, doi: https://doi.org/10.1016/j.catena.2017.06.004.

[44] D. A. Sabău, G. ŞERBAN, T. Tudose, and D. PETREA, "Correlation between precipitation and orography-key element of the Spatial Decision Support System for Prevention and Management of Floods in the Firiza Basin (Northwest Romanian Carpathians)," in *Forum Geografic*, 2022, vol. 21, no. 1, doi:

http://dx.doi.org/10.5775/fg.2022.045.i.

[45] W. Xu and E. J. Zipser, "Properties of deep convection in tropical continental, monsoon, and oceanic rainfall regimes," *Geophysical Research Letters,* vol. 39, no. 7, 2012, doi: https://doi.org/10.1029/94WR01971.

[46] Y. A. Chagati, "Study of the Conditions of Air Depressions in Determining the Intensity of Rainfalls Over Iraq," *Journal of College of Education for Pure Science,* vol. 10, no. 2, 2020, doi: https://doi.org/10.32792/jeps.v10i2.73.

[47] G. M. McFarquhar, "Rainfall microphysics," *Rainfall,* pp. 1-26, 2022, doi: https://doi.org/10.1016/B978-0-12-822544-8.00009-3.

[48] L. Wang, Y. Li, Y. Gan, L. Zhao, W. Qin, and L. Ding, "Rainfall erosivity index for monitoring global soil erosion," *Catena,* vol. 234, p. 107593, 2024, doi: https://doi.org/10.1016/j.catena.2023.107593.

[49] W. H. Wischmeier and D. D. Smith, *Predicting rainfall erosion losses: a guide to conservation planning* (no. 537). Department of Agriculture, Science and Education Administration, 1978.

[50] J. Brychta, J. Podhrázská, and M. Šťastná, "Review of methods of spatio-temporal evaluation of rainfall erosivity and their correct application," *Catena,* vol. 217, p. 106454, 2022, doi: https://doi.org/10.1016/j.catena.2022.106454.

[51] C. A. Bonilla and K. L. Vidal, "Rainfall erosivity in central Chile," Journal *of Hydrology,* vol. 410, no. 1-2, pp. 126-133, 2011, doi: https://doi.org/10.1016/j.jhydrol.2011.09.022.

[52] A. M. da Silva, "Rainfall erosivity map for Brazil," *Catena,* vol. 57, no. 3, pp. 251-259, 2004, doi: https://doi.org/10.1016/j.catena.2003.11.006.

التحليل الجغرافي المكاني لتآكل الأمطار باستخدام تقنيات الاستشعار عن بعد ونظم المعلومات الجغرافية

الملخص

تُعتبر قابلية تآكل الأمطار من حيث شدتها وطاقتها الحركية عاملاً حاسماً في تقييم مخاطر تآكل التربة في ظل استخدام الأراضي وتغير المناخ مستقبلاً. وقد استُخدمت تقنيات الاستشعار عن بُعد ونظم المعلومات الجغرافية في هذا البحث لرسم خرائط التعبير الجغرافي المكاني لقابلية تآكل الأمطار في حوض الدبس، الواقع شمال العراق، شمال غرب مدينة كركوك، بين خطي الطول ٤٣°١٠'٤٤" شرقاً و٤٤°٤٠'٦" شرقاً، وخطي العرض ٣٥°٣٠'٣٠" شمالاً و٣٥°٥٠'٠٠" شمالاً. وقد جُمعت بيانات هطول الأمطار من ثلاث محطات أرصاد جوية خلال فترة ٢٤ عاماً (٢٠٠٠-٢٠٢٤). تم استيفاء البيانات باستخدام طريقة الترجيح العكسي للمسافة (IDW) باستخدام برنامج ArcGIS الإصدار ١٠.٨.٢، وذلك لتحقيق تمثيل جغرافي مكاني لمتوسط هطول الأمطار السنوي وقابلية تآكل الأمطار في منطقة الدراسة. تراوح متوسط هطول الأمطار السنوي وقابلية تآكل الأمطار في حوض ديبس بين ٢٧٢.٥٣٧ و٣٠٢.٧٧٢ ملم، وبين ٢٤٢ و٣٣٨ $MJ.mm.ha^{-1}.h^{-1}.year^{-1}$، على التوالي. ومن خلال هذا البحث، طُوّرت صيغة جديدة لحساب قابلية تآكل الأمطار لجميع مستجمعات المياه والأحواض في العالم. ويؤكد هذا العمل على أهمية دمج بيانات المناخ والأدوات المكانية والتحليل الجيومورفولوجي لتقييم قابلية تآكل الأمطار اللازمة لتنمية وإدارة المياه والتربة والبيئة.

الكلمات الرئيسية:

نموذج الارتفاع الرقمي، نظم المعلومات الجغرافية، المسافة العكسية المرجحة، قابلية تآكل الأمطار، الاستشعار عن بعد.

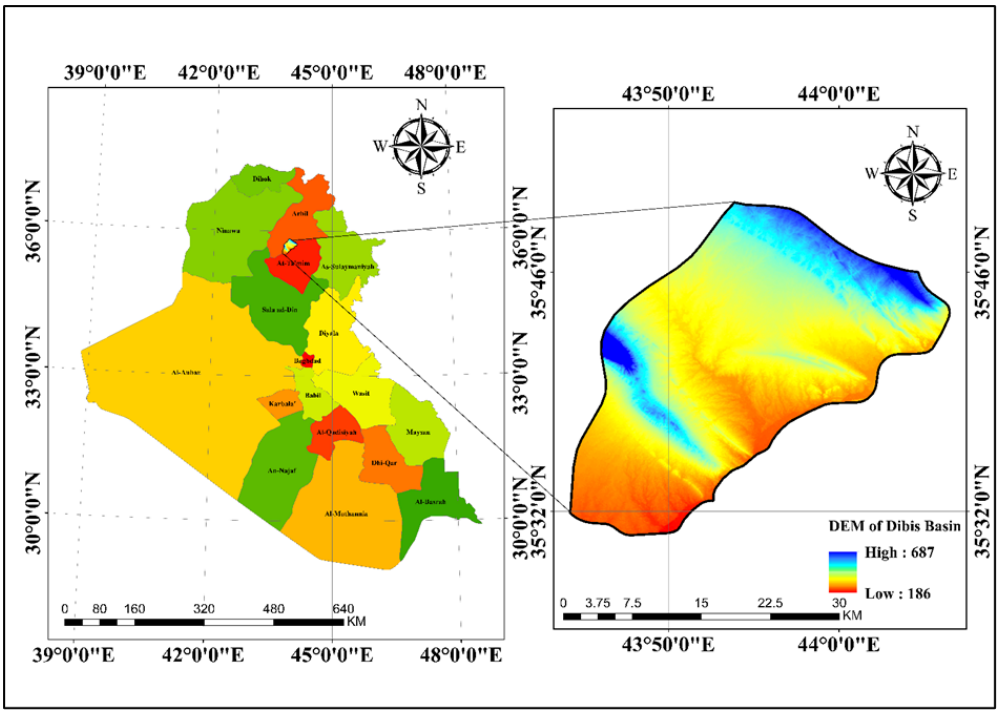

Figure 1: Location of Dibis Basin.

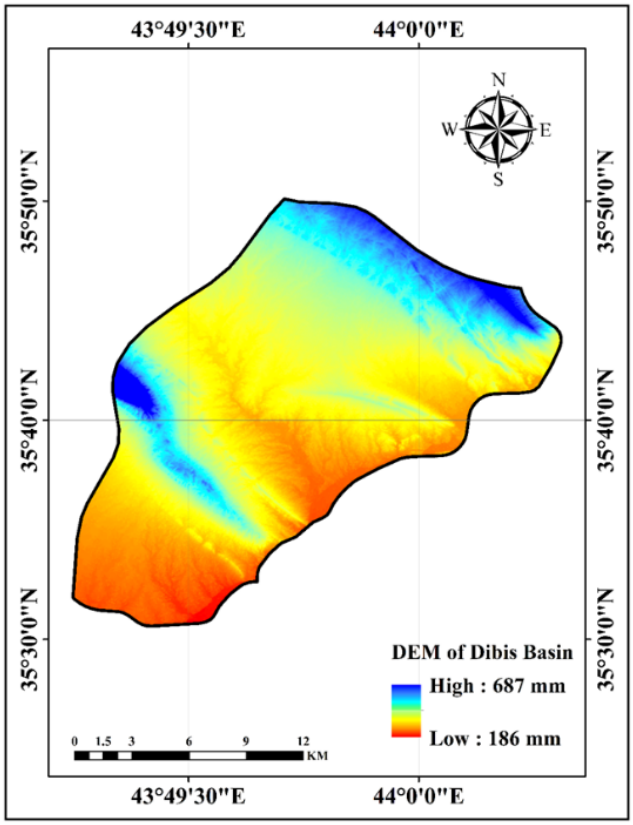

Figure 2. The DEM of Dibis Basin.

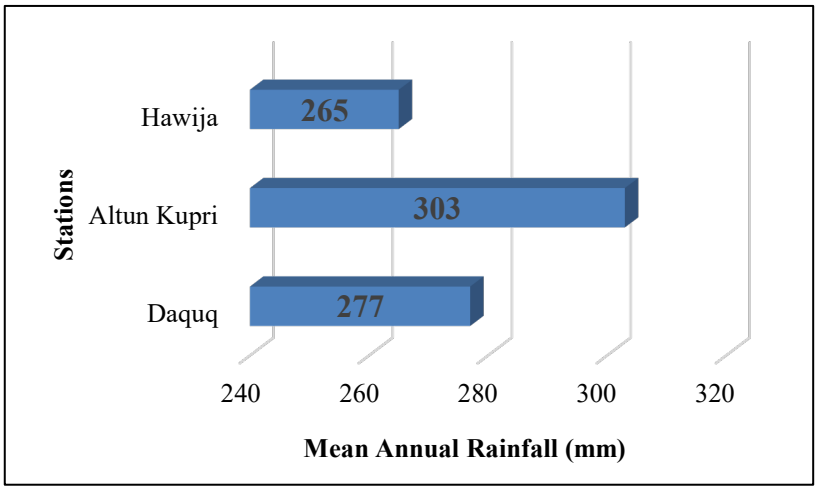

Figure 3. Mean annual rainfall for three weather monitoring station during the period (2000 to 2024).

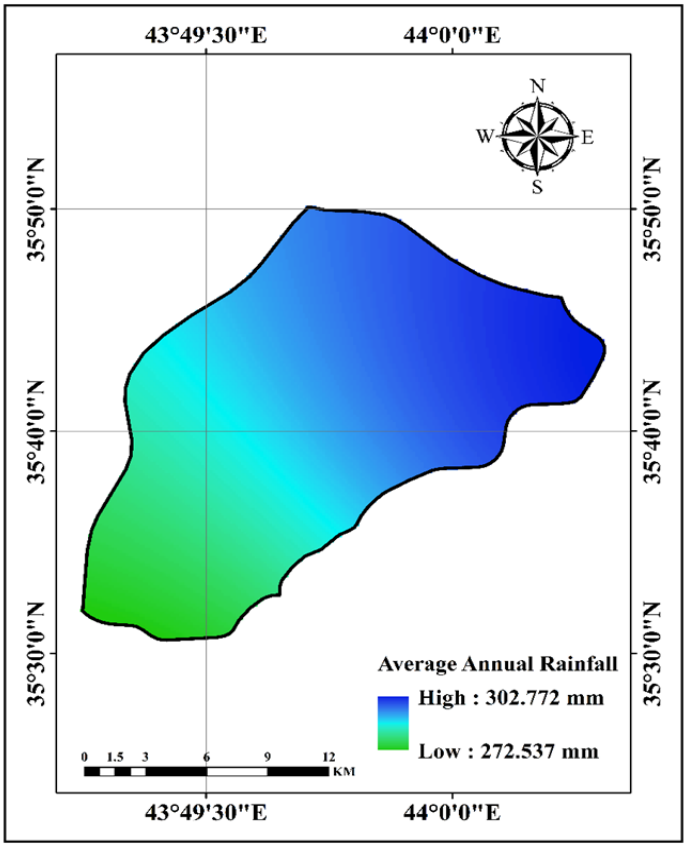

Figure 4. Geospatial representation of the mean annual rainfall of Dibis Basin.

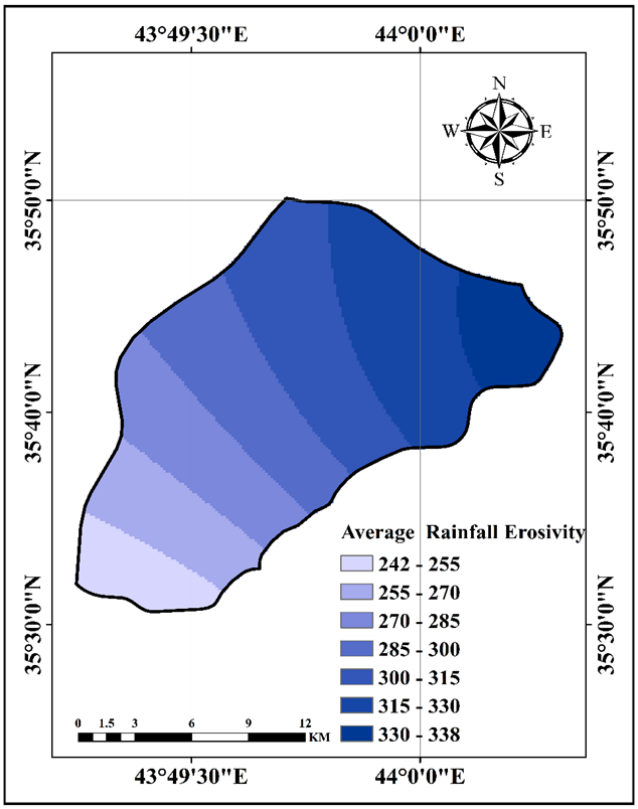

Figure 5. Geospatial representation of the rainfall erosivity of Dibis Basin.

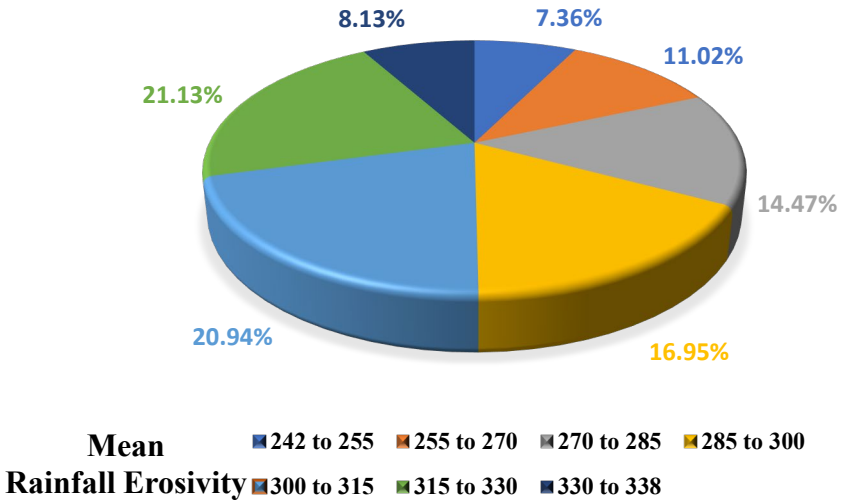

Figure 6. Distribution ratio of rainfall erosivity categories across Dibis Basin.

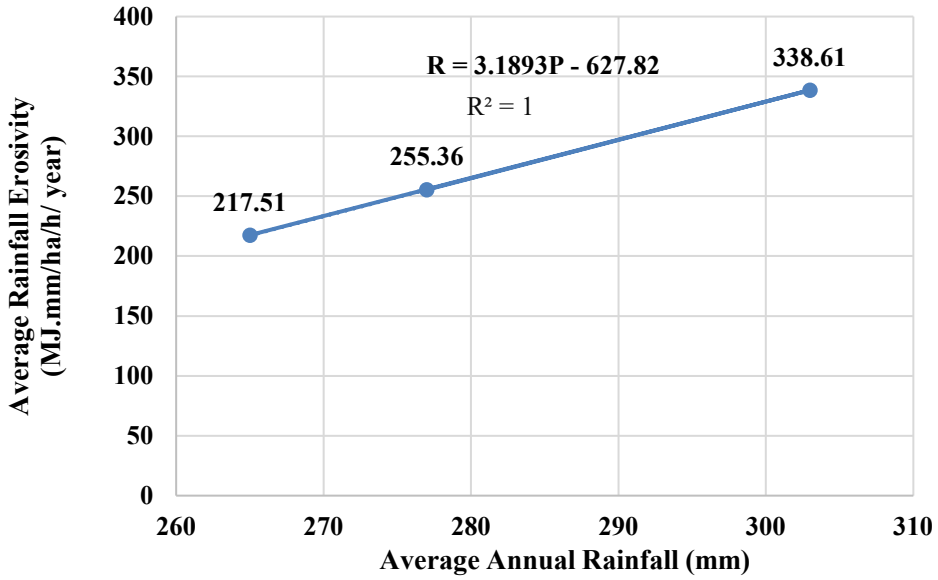

Figure 7. Bivariate relationship of mean annual rainfall and mean rainfall erosivity.

Table 1: Classification of rainfall erosivity (R) factor levels [52].

Class ID	(R) Factor Range	Classification Label
A	$R \leq 2452$	Low
B	$2452 < R \leq 4095$	Medium
C	$4095 < R \leq 7357$	Medium-Strong
D	$7357 < R \leq 9810$	Strong
E	$R > 9810$	Very Strong

Table 2: Mean annual rainfall in millimeters for each weather monitoring station over the period 2000 to 2024.

Number	Stations	Latitude (N)	Longitude (E)	Location	Mean Annual Rainfall (mm)
1	Daquq	35.1693	44.403	Kirkuk	277
2	Altun Kupri	35.73	44.15	Kirkuk	303
3	Hawija	35.3	43.76	Kirkuk	265

Table 3: Rainfall Erosivity of Dibis Basin according to utilizing equations.

Number	Stations	Rainfall Erosivity Applying the Method of (Renard and Freimund)	Rainfall Erosivity Applying the Method of (Saber and Suleiman)	Rainfall Erosivity Applying the Method of (Yu and Rosewell)	Rainfall Erosivity Applying the Method of (Ferrari et al)	Mean Rainfall Erosivity
1	Daquq	413.37	79.36		153.88	255.36
2	Alton-kobri	477.61	184.79	374.85	258.95	338.61
3	Hawija	384.92	30.70	433.11	105.38	217.51

Table 4: Mean rainfall erosivity values by classification within the Dibis Basin.

Number	Mean Rainfall Erosivity	Rainfall Erosivity Class	Area %	Area in Km^2
1	242 to 255	Low Rainfall Erosivity	7.3602%	48.4447
2	255 to 270	Low Rainfall Erosivity	11.0281%	72.5871
3	270 to 285	Low Rainfall Erosivity	14.4653%	95.2106
4	285 to 300	Low Rainfall Erosivity	16.9491%	111.5586
5	300 to 315	Low Rainfall Erosivity	20.9449%	137.8595
6	315 to 330	Low Rainfall Erosivity	21.1271%	139.0586
7	330 to 338	Low Rainfall Erosivity	8.1253%	53.4809